The Vertical Structure of North Pacific Temperature Anomalies

KIRK BRYAN

Geophysical Fluid Dynamics Laboratory/NOAA, Princeton, New Jersey 08540

P. RIPA[1]

Princeton University, Princeton, New Jersey 08540

The existence of large-scale thermal anomalies in the North Pacific motivates a study of the reflection of a wind-driven anomaly at the eastern boundary. A continuously stratified, linear model is used to calculate the vertical and horizontal structure of large-scale waves forced by fluctuating wind stress patterns. Thermal anomalies caused by eastward, westward, and standing wind wave patterns are investigated. Although exact comparison with data is not possible, the model can predict downward phase propagation as observed at OWS station N without invoking friction or vertical mixing of heat. In the same solution, upward propagation is predicted at other locations. An eastward moving, forced anomaly in the thermocline transports energy toward the eastern boundary. In the model the anomaly is reflected at the wall in the form of westward moving, internal Rossby waves which have a much lower group velocity. A small amount of friction will attenuate the outgoing waves much more than the incoming waves, providing a mechanism for eastward intensification.

INTRODUCTION

The difference between the monthly sea surface temperature averaged over many years and the monthly sea surface temperature observed in any given year amounts to 1–2°C. *Namias* [1973] has drawn attention to these anomalies which are coherent over a large part of the North Pacific in mid-latitudes. The anomalies may also persist for several years. A statistical analysis of the temperature anomalies by *Davis* [1976] shows that the amplitude of the leading empirical orthogonal component of sea surface temperature in the North Pacific has a 'red' spectrum. That is, the variance is inversely proportional to frequency out to the low-frequency limit that can be resolved by the limited time series available. Davis also concludes that the anomalies generally drift eastward, although exceptions exist in the data. The eastward drift was pointed out in an earlier study by *Favorite and McLain* [1973].

A map of temperature anomaly averaged over an entire year is shown in Figure 1, taken from a paper by *White* [1975]. The map illustrates the spectacularly large scale of the phenomenon. Evidence for vertical penetration was noted some years ago by *Fofonoff and Tabata* [1966] based on an analysis of data at OWS station P in the northeastern Pacific. Results from a more recent study of a longer time series are shown in Figure 2*a*. [*White and Walker*, 1974]. Also included, in Figure 2*b*, is a map of the location of three ocean weather ship stations for which temperature profile time series are available. White and Walker found that the surface anomalies penetrated to at least 250 m in the North Pacific. (An appropriate generic name for this phenomenon is 'jerwarbuz,' in honor of the pioneering work of J. Namias, W. A. White, and R. Bernstein.) A low-pass record from which all frequencies of 1 cpy or greater have been removed is shown in Figure 2*a*. The temperature anomaly data are from OWS station P and are presented in the form of a *z-t* plot for the years 1950–1969. The low-pass data show dominant contributions of periods of 5–6 years. *White and Walker* [1974] point out that the patterns in Figure 2*a* are systematically tilted, indicating downward phase propagation. A similar feature is present at OWS station N to the south. The downward phase propagation amounts to approximately 100 m/yr. To the authors' knowledge, no serious attempts have been made to explain this puzzling feature.

The present study is partly motivated by the evidence for downward phase propagation in Figure 2*a*. A highly idealized model is considered. No pretense is made of directly modeling the complex process which may ultimately generate the North Pacific anomalies. Indeed, such an effort would be premature in view of the small amount of data available at the present time. More detailed modeling must await the results of a large-scale field program under Norpax which is presently being carried out. (Norpax is a cooperative field program sponsored by the International Decade of Ocean Exploration Program of the National Science Foundation and the U.S. Navy.) In this paper a simple generating mechanism is assumed which causes the anomalies to form as a standing wave or drift eastward. Attention is focused on the reflection of the anomalies at the eastern boundary. The present study may be considered an extension of a pioneering paper by *White* [1977], in which he finds evidence for planetary baroclinic Rossby waves generated at the eastern boundary of the tropical North Pacific. In this paper the same idea is extended to the lower frequencies associated with the mid-latitude North Pacific temperature anomalies. A continuously stratified model allows us to examine the vertical structure associated with the forced and free waves.

Solutions are obtained from a boundary condition at the eastern wall appropriate for low frequencies, making use of a linearized quasi-geostrophic model. Since the eastward drift of the anomalies is actually larger than the rather sluggish mean currents of the eastern North Pacific, the effect of mean currents is omitted in the model. More rapid currents occur in the California Current, but it occupies an area relatively small in comparison to the large-scale anomalies under consideration. There is only a narrow shelf along the Pacific coast of North America which makes the abrupt wall in the model a reasonable assumption. To simplify our solutions, only one frequency is considered at a time, keeping in mind that solutions for many frequencies can be superimposed to fit more accurately the broadbanded phenomena actually observed.

[1] Now at PMEL/NOAA, University of Washington, Seattle, Washington 98105.

Paper number 7C0966.
0148-0227/78/057C-0966$03.00

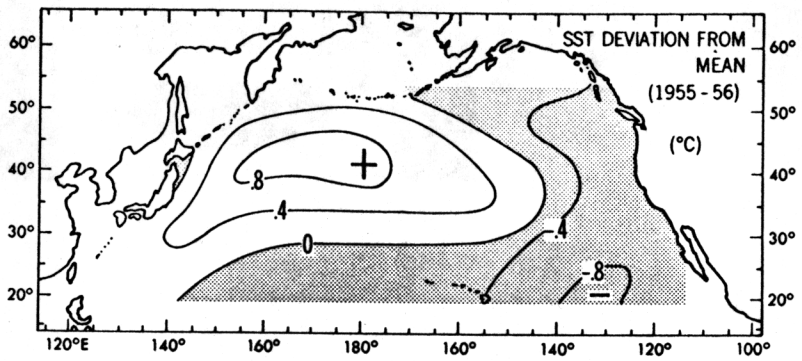

Fig. 1. Sea surface temperature anomaly for the years 1955–1956 [from *White*, 1975].

In a recent study [*Hasselmann and Frankignoul*, 1977] an interesting mechanism is proposed for the generation of North Pacific anomalies. *Hasselmann and Frankignoul* [1977] note that a random process like atmospheric cyclones has energy distributed through all frequencies. Even though the wind energy at low frequencies is relatively small, the authors point out that the ocean response greatly amplifies the lowest frequencies. *Hasselmann and Frankignoul* [1977] assume that an unspecified oceanic feedback keeps temperature anomalies bounded at very low frequencies (less than 0.1 cpy).

The observed fact that surface temperature anomalies drift eastward suggests that an eastward moving wind pattern is a dominant generating mechanism for the North Pacific temperature anomalies. On the other hand, a recent statistical analysis of the surface wind data by *Barnett* [1977] suggests that much of the variance at low frequencies may be localized in the eastern part of the North Pacific. In the present study both types of wind patterns are considered. In one case a train of cyclonic and anticyclonic gyres moving eastward generates upward and downward displacements of the thermocline, which also move eastward lagging 90° in phase behind the wind pattern. In a second case, a westward moving wind pattern of equal amplitude is added to the eastward wind pattern to form a standing wave pattern.

The base state of the ocean is a horizontally uniform stratification. The density profile has the same mathematical form as that used by *Garrett and Munk* [1972] in their model of internal gravity wave spectra. Density is uniform in an upper mixed layer and has an exponential profile in the main thermocline, becoming nearly uniform below 2 km. Except in the deep water the model can provide a reasonable fit to North Pacific data with the proper choice of constants.

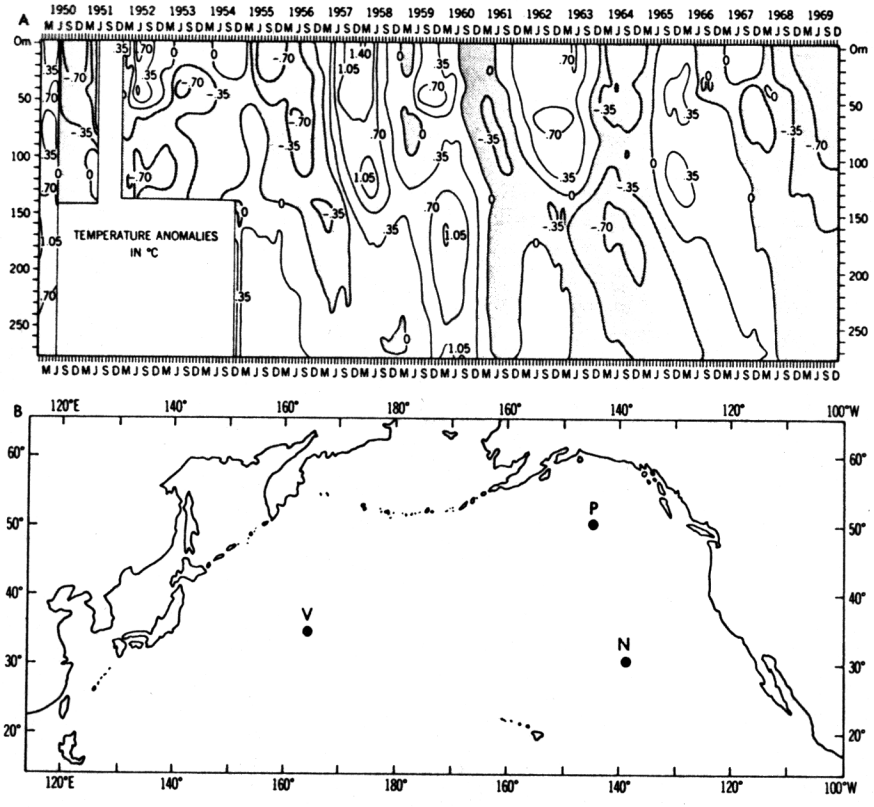

Fig. 2. (*a*) A 12-month running mean of the temperature anomalies based on bathythermograph data from OWS *Papa* [from *White and Walker*, 1974]. (*b*) The location of ocean weather stations in the North Pacific.

MODEL

As was indicated in the introduction, mean currents and horizontal density gradients are neglected to first order. The governing equations for momentum and continuity are

$$\partial_t u - fv + \rho_0^{-1}\partial_x p = X \tag{1}$$

$$\partial_t v + fu + \rho_0^{-1}\partial_y p = Y \tag{2}$$

$$\rho g + \partial_z p = 0 \tag{3}$$

$$\partial_z w + \partial_x u + \partial_y v = 0 \tag{4}$$

X and Y are body forces which represent the divergence of the vertical eddy flux of momentum. They are assumed to be vertically uniform in a shallow mixed layer and to be zero in the main thermocline.

Density is also assumed to be uniform in a shallow mixed layer but varies according to an exponential law below

$$\begin{aligned} \tilde{\rho} &= \rho_0 \qquad 0 > z > -h \\ \tilde{\rho} &= \rho_0 + (\rho_0/\gamma g)N^2(0)(e^{-\gamma h} - e^{\gamma z}) \qquad -h > z > -H \end{aligned} \tag{5}$$

The density profile is fairly realistic for the eastern North Pacific. For uniform stratification in the horizontal plane the governing equation for density is

$$\partial_t \rho - N^2\rho_0 w/g = 0 \tag{6}$$

The geometry of the model is a semi-infinite, beta plane at mid-latitudes with a wall at the eastern boundary. At the eastern wall we require that the normal component of velocity vanish. The rigid lid approximation also requires the normal component of velocity to vanish at the upper and lower boundaries.

$$u = 0 \qquad x = 0 \tag{7}$$

$$w = 0 \qquad z = 0, -H \tag{8}$$

Taking the derivative with respect to x of (2) and subtracting the derivative with respect to y of (1), we obtain

$$\partial_t(\partial_x v - \partial_y u) - f\partial_z w + \beta v = \partial_x Y - \partial_y X \tag{9}$$

Differentiating (6) with respect to z and substituting from the hydrostatic equation, we obtain

$$\partial_z w = -\partial_t\partial_z[(N^2\rho_0)^{-1}\partial_z p] \tag{10}$$

The geostrophic relation is

$$f(u, v) = -\rho_0^{-1}(\partial_y p, -\partial_x p) \tag{11}$$

In the mixed layer, (11) and (9) may be combined to give

$$\partial_t \Delta p - f^2\rho_0\partial_z w + \beta\partial_x p = f\rho_0(\partial_x Y - \partial_y X) \tag{12}$$

Below the mixed layer, X and Y are zero. Combining (9) and (11) gives

$$\partial_t(\Delta p - \lambda^2 p) + \beta\partial_x p = 0 \tag{13}$$

where

$$\partial_z(f^2/N^2)\partial_z p + \lambda^2 p = 0 \tag{14}$$

We assume that the pattern of wind forcing has the form

$$X, Y = (\hat{X} \sin ly, \hat{Y} \cos ly) \exp[i(k_f x - \omega t)] \tag{15}$$

The solution is made up of two parts, a forced solution moving at the speed ω/k_f of the wind pattern and a free solution needed to satisfy boundary conditions at the eastern wall:

$$p = \alpha_f[\hat{p}_f(z) \cos ly \exp[i(k_f x - \omega t)] + \sum_{n=0}^{\infty} \alpha_n \hat{p}_n(z) \cos ly \exp[i(k_n x - \omega t)] \tag{16}$$

Substituting the solution (16) in (13), we obtain for the forced waves

$$\lambda_f^2 = -k_f\beta/\omega - k_f^2 - l^2 \tag{17}$$

Equation (17) determines λ_f^2 in terms of known quantities. Once λ_f^2 is determined, the forced solution $\hat{p}_f(z)$ can be found from (14) and appropriate boundary conditions. On the other hand, the frequency equation corresponding to free Rossby waves is

$$k_n^2 + l^2 + \lambda_n^2 = -k_n\beta/\omega \tag{18}$$

there $\lambda_n (n = 0, 1, 2, \cdots)$ are the eigenvalues of the normal modes of the specified vertical density profile. In the next section we will show how λ_n is determined independently of (18), allowing us to use (18) as a means of finding $k_n (n = 0, 1, 2, \cdots)$ for each normal mode.

For periods greater than 1 year and horizontal scales greater than 1000 km, $\beta/\omega \gg |k|$. Thus for our case, (17) and (18) can be accurately approximated by

$$\lambda_f^2 = -k_f\beta/\omega \tag{19}$$

and

$$k_n = -\lambda_n^2\omega/\beta \tag{20}$$

Note that λ_f^2 must be negative for an eastward forced wave and positive for a westward forced wave. Parameter λ_n^2 is positive for the normal modes which always move westward. In the next section we will consider the vertical displacement profiles of the free and forced waves.

VERTICAL PROFILES

The density profile used is like one profile considered by *Garrett and Munk* [1972]. It is convenient to work in terms of vertical velocity rather than pressure, owing to the simpler boundary conditions. Let

$$\hat{p} = d_z\hat{w} \tag{21}$$

where $\hat{w} = 0$ at $z = 0, -H$, except for an external mode which is independent of z. Corresponding to (14) we have

$$d_z d_z\hat{w} + N^2\lambda^2\hat{w}/f^2 = 0 \tag{22}$$

We note that $N^2(z) = N(0)^2 \exp(\gamma z)$ below the thermocline. When a new variable $s = \exp(\gamma z/2)$ is introduced, (22) becomes

$$s^2\hat{w}'' + s\hat{w}' + s^2\mu^2\hat{w} = 0 \tag{23}$$

where

$$\mu^2 = [2N(0)\lambda/f\gamma]^2 \tag{24}$$

Equation (23) is a standard Bessel equation. For $\mu^2 > 0$, (23) is satisfied by zero-order Bessel functions of the first and second kind:

$$\hat{w}_n = c_n\mathcal{C}_0(\mu_n s) = c_n[J_0(\mu_n s) + b_n Y_0(\mu_n s)] \tag{25}$$

and $n = 1, 2, 3, \cdots$. Above the thermocline, in the mixed layer, $N^2 = 0$, and (22) becomes

$$d_z d_z\hat{w} = 0 \tag{26}$$

For free waves, $\hat{w}$ and $d_z\hat{w}$ must be continuous at the base of the mixed layer. Let $s^* = \exp(-\gamma h/2)$ and $\epsilon = \exp(-\gamma H/2)$:

$$\begin{aligned} \hat{w}_n &= -zc_n\mathcal{C}_0(\mu_n s^*)/h \qquad z > -h \\ \hat{w}_n &= c_n\mathcal{C}_0(\mu_n s) \qquad z < -h \end{aligned} \tag{27}$$

To insure that $\hat{w}$ vanishes at $z = -H$,

$$b_n = -J_0(\mu_n\epsilon)/Y_0(\mu_n\epsilon) \tag{28}$$

The condition that the vertical derivative be continuous at the interface,

$$\mathcal{C}_0(\mu_n s^*) = -(\gamma h/2)s^*\,\mathcal{C}_0'(\mu_n s^*) \tag{29}$$

determines the eigenvalue, μ_n. We can normalize the $\hat{w}_n$'s such that

$$(\gamma/2N_0)\int_{-H}^{0} \hat{w}_n\hat{w}_m N\,dz = \int_{\epsilon}^{s^*} \hat{w}_n\hat{w}_m\,s\,ds = 1 \qquad m = n$$

$$(\gamma/2N_0)\int_{-H}^{0} \hat{w}_n\hat{w}_m N\,dz = \int_{\epsilon}^{s^*} \hat{w}_n\hat{w}_m\,s\,ds = 0 \qquad m \neq n \tag{30}$$

The normalizing constant is

$$1/c_n^2 = (s^2/2)(\mathcal{C}_0^2 + \mathcal{C}_0'^2/\mu_n^2)\Big|_{\epsilon}^{s^*} \tag{31}$$

Forced waves for which $\mu^2 < 0$ must be written in terms of modified Bessel functions:

$$\hat{w}_{f+} = \mathcal{D}_0(\mu_f s) = I_0(\mu_f s) + b_f K_0(\mu_f s) \tag{32}$$

In the mixed layer the forced wave is also proportional to z:

$$\hat{w}_{f+} = -z\mathcal{D}_0(\mu_f s^*)/h \qquad z > -h$$

$$\hat{w}_{f+} = \mathcal{D}_0(\mu_f s) \qquad z < -h \tag{33}$$

Parameter b_f is determined by a relation parallel to (28). w_{f+} is the forced wave associated with the eastward moving wind component.

Next, we consider the component associated with the westward wind component, w_{f-}. In this case, $\mu^2 > 0$.

$$\hat{w}_{f-} = C_{f-}\mathcal{C}_0(\mu_f s) = C_{f-}[J_0(\mu_f s) + b_{f-}Y_0(\mu_f s)] \tag{34}$$

The coefficient C_{f-} is taken to be

$$C_{f-} = \mathcal{D}_0(\mu_f s^*)/\mathcal{C}_0(\mu_f s^*) \tag{35}$$

so that $\hat{w}_{f+} = \hat{w}_{f-}$ at $z = h$. Within the mixed layer the profiles of $\hat{w}_{f-}$ and $\hat{w}_{f+}$ are identical.

Reflected Baroclinic Waves at the Eastern Boundary

It is shown in appendix A that for frequencies less than 1.0 cpy a geostrophic boundary condition is a reasonable approximation at the eastern wall. For the condition of no normal flow through the eastern wall to be satisfied the eastern boundary must coincide with a stationary nodal line in the perturbation pressure field. Thus at $x = 0$ the free and forced solutions must match exactly. Setting the left-hand side of (16) equal to zero gives

$$\sum_{n=0}^{\infty} \alpha_n\hat{p}_n(z) = -\hat{p}_f(z) \tag{36}$$

Replacing $\hat{p}(z)$ with $d_z\hat{w}$ from (21) and integrating the resulting equation with respect to z, we obtain

$$\sum_{n=1}^{\infty} \alpha_n\hat{w}_n = -\hat{w}_f \tag{37}$$

We make the rigid lid approximation in our model which excludes the zeroth mode from the w field.

To relate the vertical velocity to the wind, we note that a good approximation to the forced upwelling at the base of the mixed layer is equal to the divergence of the Ekman transport. Thus

$$\frac{w(-d)}{\hat{w}(-d)} \simeq \frac{(\partial_x Y - \partial_y X)h}{f\mathcal{D}_0(\mu_f s^*)}$$

Multiplying both sides of (37) by $\hat{w}_n s$ and integrating with respect to s from ϵ to s^*, we obtain after making use of the orthogonality condition (30),

$$\alpha_n = -\int_{\epsilon}^{s^*} \hat{w}_f\hat{w}_n s\,ds \tag{38}$$

If we substitute the analytic expressions for $\hat{w}_f$ and $\hat{w}_n$ given in the previous section, (38) can be evaluated from integral tables [*Abramowitz and Stegun*, 1964, p. 484]. For the eastward part,

$$\alpha_{n+} = \frac{c_n[s(\mathcal{C}_0'\langle\mathcal{D}_0\rangle - \langle\mathcal{D}_0'\rangle\mathcal{C}_0)\,|_{\epsilon}^{s^*}]}{\mu_n^2 + \mu_f^2} \tag{39}$$

and for the westward part,

$$\alpha_{n-} = \frac{C_{f-}c_n[s(\mathcal{C}_0'\langle\mathcal{C}_0\rangle - \langle\mathcal{C}_0'\rangle\mathcal{C}_0)\,|_{\epsilon}^{s^*}]}{\mu_n^2 - \mu_f^2} \tag{40}$$

where the angle brackets indicate the forced solution.

The parameter values given in Table 1 serve as a basis for computing a realistic case to illustrate the solution. We choose a period of 6 years based on the longest dominant time scale shown in the OWS station P record of Figure 2*a*. The horizontal wavelength of about 10,000 km corresponds to the size of the anomalies shown in Figure 1. Other values are chosen to correspond to the North Pacific at mid-latitudes. One exception is the choice of a mixed layer depth of 100 m, which is rather deep for this region of the world ocean.

In order to determine the density patterns associated with the forced mode we note that the shape profiles for density are proportional to the product of the vertical velocity multiplied by N^2 from (6),

$$(\hat{\rho}_f, \hat{\rho}_n) = N^2(\hat{w}_f, \hat{w}_n) \tag{41}$$

Substituting the analytic expressions for $\hat{w}_{f+}$ and $\hat{w}_n$, we obtain

$$(\hat{\rho}_f, \hat{\rho}_n) = N^2\{\mathcal{D}_0[\mu_f \exp(\gamma z/2)],\ c_n\mathcal{C}_0[\mu_n \exp(\gamma z/2)]\} \tag{42}$$

Combining (19) and (20) with (24), we obtain long-wave approximations for μ_f^2 and μ_n^2:

$$\mu_f^2,\ \mu_n^2 = [2N(0)/f\gamma]^2(-k_f\beta,\ -k_n\beta)/\omega \tag{43}$$

Note that μ_f^2 is inversely proportional to ω/k_f. As a result, the forced density perturbation is more and more trapped at the surface for lower and lower frequencies for a given k_f. This effect is illustrated in Figure 3, in which the vertical profiles of the eastward forced wave are plotted for three different frequencies. The result corresponds to the original ideas about the adjustment of a baroclinic ocean to variable wind [*Veronis and Stommel*, 1956]. The degree of trapping in the upper ocean shown in Figure 3 is a measure of baroclinic adjustment to a moving wind pattern. The lower the frequency of the eastward propagating wind pattern the greater the baroclinic adjustment will be.

Density profiles associated with the first three normal modes are shown in Figure 4. Characteristic wave numbers and phase speeds calculated from (43) are shown in Table 2. Also shown is the percentage of variance of the forced mode explained by each of the free baroclinic modes in the interval $-h > z > -H$. Note that the speed of the incoming wave is much greater than the phase velocity of the westward propagating modes. Since

TABLE 1. Numerical Values of the Parameters for the Case Shown in Figures 5 and 6 and Table 2

Parameter	Description	Value
β	beta	1.6×10^{-11} (ms)$^{-1}$
f	Coriolis parameter	10^{-4} s^{-1}
$2\pi/k_f$	E-W wavelength (forced mode)	9461 km
$2\pi/l$	N-S wavelength (forced mode)	6000 km
$2\pi/\omega$	period	6 years
$2\pi/N(0)$	Brunt-Väisälä period	9.3 min
$1/\gamma$	e folding depth	400 m
h	depth of mixed layer	100 m
H	total depth	5 km

these waves are approximately nondispersive, there is a similar difference in the group velocities of the incoming and outgoing waves. Friction is omitted in the model, but it must be present in the real ocean. The scattered waves with lowest group velocity will "age" before they can penetrate very far into the interior of the basin. On the assumption that attenuation by friction will be proportional to time the highest modes will only be able to go a short distance from the wall. The first baroclinic mode will be least affected by friction because of its higher group velocity. Friction would provide a mechanism for energy accumulation at the eastern wall. The mechanism is, in some ways, analogous to *Pedlosky*'s [1965] theory for western intensification. In Pedlosky's mechanism both the incoming and outgoing waves have a westward phase velocity, but the reflected waves have a group velocity to the east which is much less than that of the incoming waves.

Density anomalies are proportional to the total displacement multiplied by N^2:

$$\rho \sim N^2 \cos ly \left[\hat{w}_f \exp(ik_f x) - \sum_{n=1}^{\infty} \alpha_n \hat{w}_n \exp(ik_n x) \right] e^{-i\omega t} \quad (44)$$

A plot of the density anomaly as a function of z and t for $x = -1800$ km is shown in Figure 5. Only eastward forcing is considered. This position roughly corresponds to that of OWS station N relative to the coast of Baja, California (see Figure 2*b*). Note that the density anomaly shown in Figure 5 indicates a systematic tilt in the z-t plane, indicating downward phase

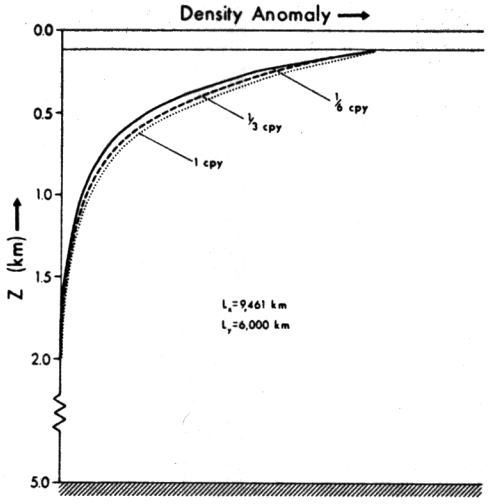

Fig. 3. Vertical profiles of the density anomaly corresponding to the forced eastward component of the analytic solution.

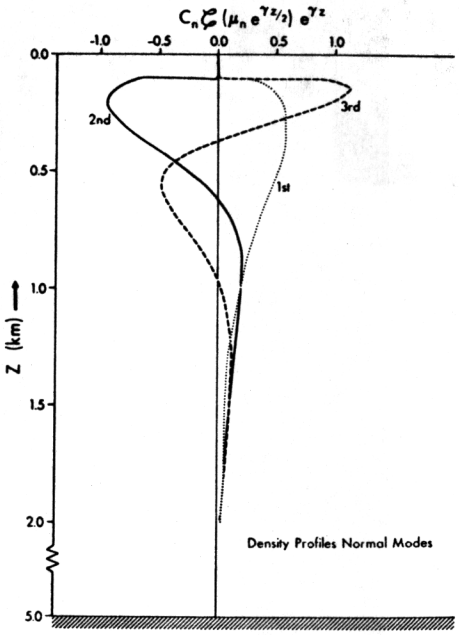

Fig. 4. Vertical profiles of the displacement corresponding to the free westward propagating waves.

propagation. The apparent propagation is fairly close to the apparent downward penetration of 100 m/yr cited by *White and Walker* [1974] for OWS stations N and P. A more complete picture of the solution with eastward forcing is given in Figure 6, which shows the amplitude and phase of the density anomaly in the x-z plane for a distance of 4000 km from the eastern boundary. Smoother patterns of amplitude and phase would be expected if some frictional damping of the westward propagating free waves were taken into account. The higher modes propagate so slowly that even a very modest linear damping will wipe them out before they penetrate more than a few hundred kilometers out from the eastern wall.

Note that the contribution of the forced wave in Figure 6 makes the amplitude largest near the surface. The matching of forced and free solutions at the eastern wall creates a significant horizontal gradient over a distance of 500 km from the boundary. From geostrophic considerations we would expect this to be associated with a meridional current which will be directed to the south for an incoming warm anomaly and to the north for an incoming cold anomaly. In the North Pacific this mechanism might provide variations in the strength of the California Current on time scales longer than 1 year. Lines of

TABLE 2. Eigenvalues and Corresponding Wavelengths and Phase Speeds for the Forced and Free Modes

Mode	$\lvert\mu\rvert$	Speed, km/d	Wavelength, km	Percent Variance
Forced	1.61	4.32	9461	
First	2.70	−1.52	3364	73
Second	5.97	−0.31	688	18
Third	9.31	−0.13	283	5
Fourth	12.73	−0.06	151	2
Total				$\sum_{1}^{4} = 98$

The period is 6 years. Also shown is the percent variance explained by each free mode when projected on the forced mode at $x = 0$. Only the eastward component of the forced wave is considered.

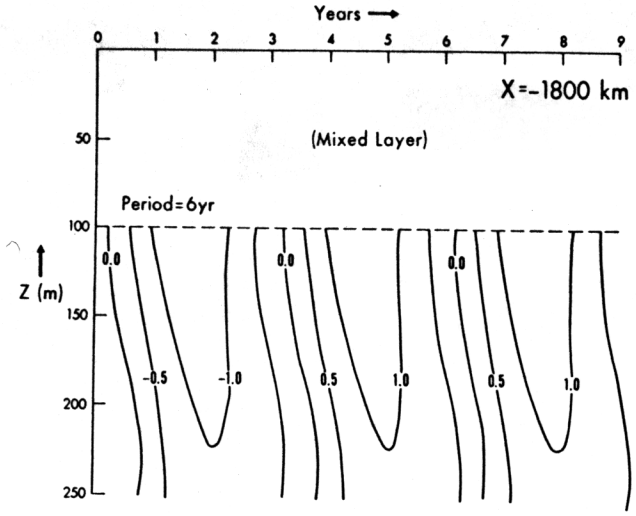

Fig. 5. Density anomalies at $x = -1800$ km computed from the analytic solution. Note the apparent downward propagation. The input corresponds to an eastward moving wind pattern.

constant phase reflect the relatively rapid propagation of the forced wave which has its greatest amplitude near the surface and the much slower propagation of the free modes which make their largest contribution to the total amplitude at depth. Note that there is an amphidromic point at about 2500 km from the eastern boundary with a clockwise phase propagation around it. Differences in horizontal phase propagation provide a completely nonlocal mechanism for downward and upward penetration of the anomalies. The predicted penetration is downward at $x = -2000$ km but upward further to both the east and the west.

The observed pattern of temperature anomaly shown in Figure 2*a* is dominated by periods of 5–7 years, but it is interesting to see what the theory predicts for a somewhat higher frequency. A solution is plotted in Figure 7 for $\omega = \frac{1}{3}$ cpy. The vertical structure of the incoming wave is changed in relation to Figure 6. It becomes deeper, as is shown in Figure 3. Since the phase velocity of the scattered Rossby waves, ω/k_n, remains fixed for different frequencies, the horizontal wave numbers are double those of the case shown in Figure 6. The result is a corresponding compression of the east-west scale. The first amphidromic point is only 1500 km removed from the eastern boundary instead of 2500 km, as in the previous case.

For with a given distance x from the eastern boundary the amphidromic point will correspond with critical frequencies ω_j defined by

$$\omega_j = 2\pi j C_1/x \tag{45}$$

where C_1 is the speed of the first baroclinic mode and j is an integer. The change in position of amphidromic points with frequency should cause a signature in the long-term temperature records of OWS stations N and P. Averaging 50-m depth intervals together, we examined an 18-year record and a 24-year record from OWS stations P and N, respectively. The vertical coherence at station N at all levels is too poor to compute phase angles with any statistical significance. Coherence at OWS station P is also low except between the temperatures averaged over the 150- to 200-m interval and the 200- to 250-m interval. The results for these depth intervals are shown in Figure 8. As is indicated in Figure 2*a*, the upper layer leads the lower layer at low frequencies. A phase difference of 30°/50 m is equivalent to *White and Walker*'s [1974] estimate of vertical propagation of 100 m/yr at a frequency of $\frac{1}{6}$ cpy. Note

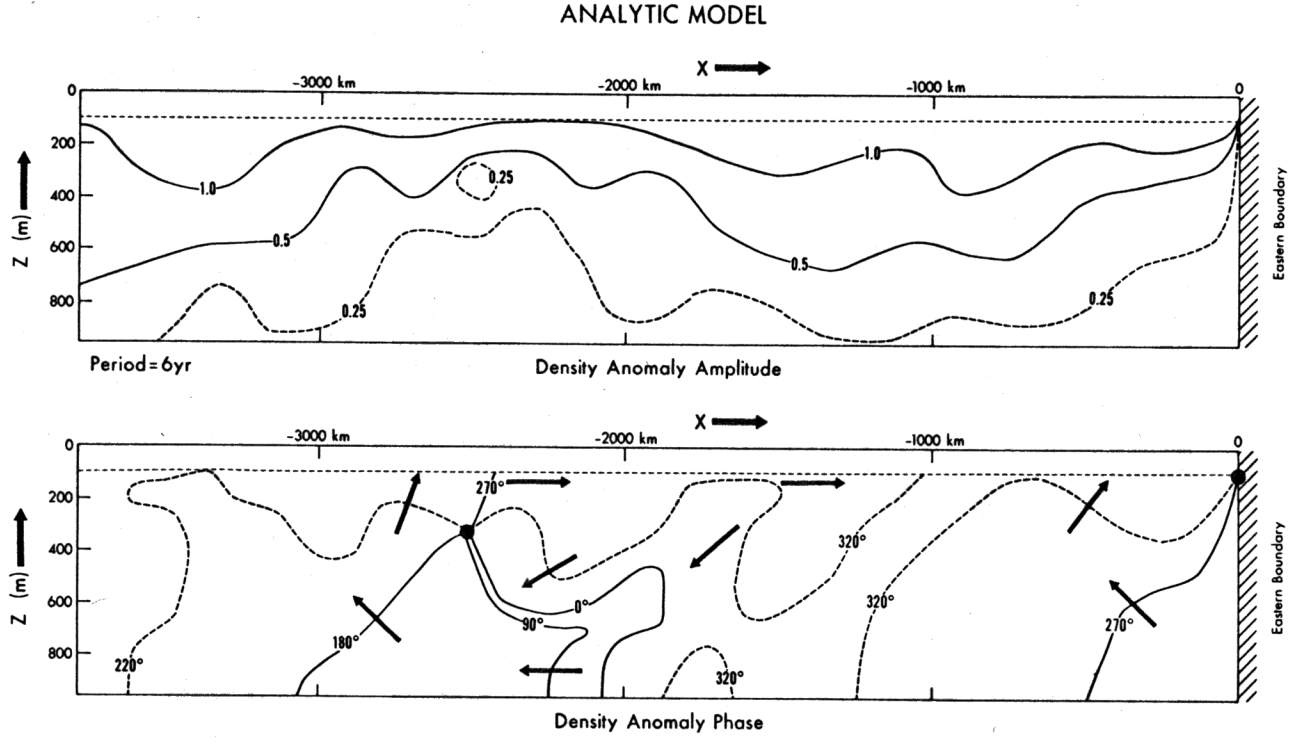

Fig. 6. (Top) Amplitude and (bottom) phase of the density anomaly of the solution. The pattern corresponds to a period of 6 years. Units of amplitude are arbitrary. The density anomaly is actually zero from 100 m to the surface, since the stratification is zero in the mixed layer. Only eastward forcing is considered.

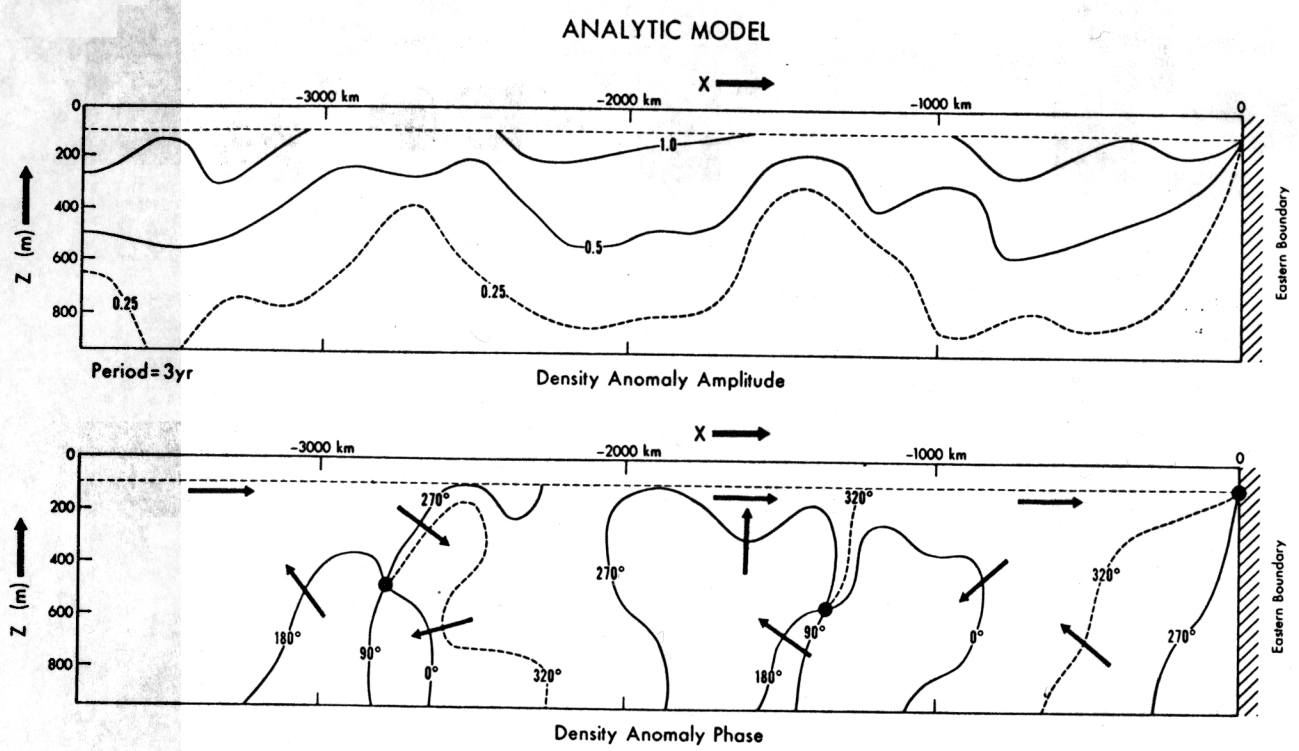

Fig. 7. Same as Figure 6 for a period of 3 years.

that for frequencies less than ½ cpy the phase tends to oscillate around zero at an irregular frequency interval. The critical frequencies for phase reversals are shown by arrows based on the speed of the first baroclinic mode given in Table 2 with a small correction for the latitude of OWS station P. Taking into account that other processes caused by different types of wind patterns and vertical mixing also influence the temperature record, the data neither prove nor disprove the existence of reflected baroclinic waves. A more precise check must await longer records which will allow higher resolution in frequency, and we need detailed data on the wind input.

Next, we consider the predicted response to a westward moving wind pattern. If the eastward and westward components are incoherent, they will act independently. The pat-

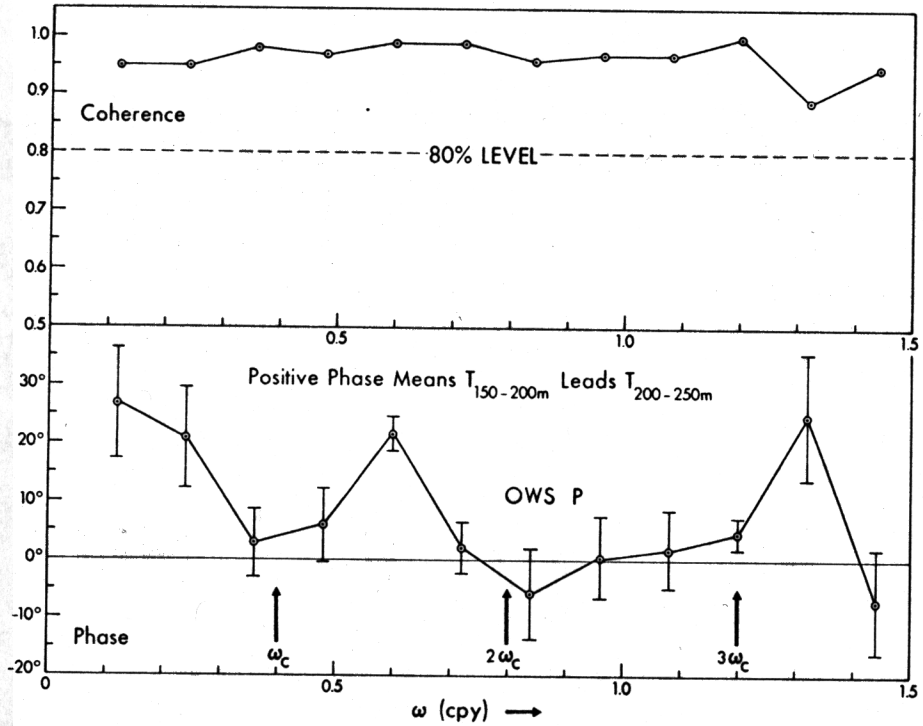

Fig. 8. Coherence and phase of the temperature averaged from 150 to 200 m versus the temperature averaged from 200 to 250 m at OWS station P. The record extends from 1950 to 1969.

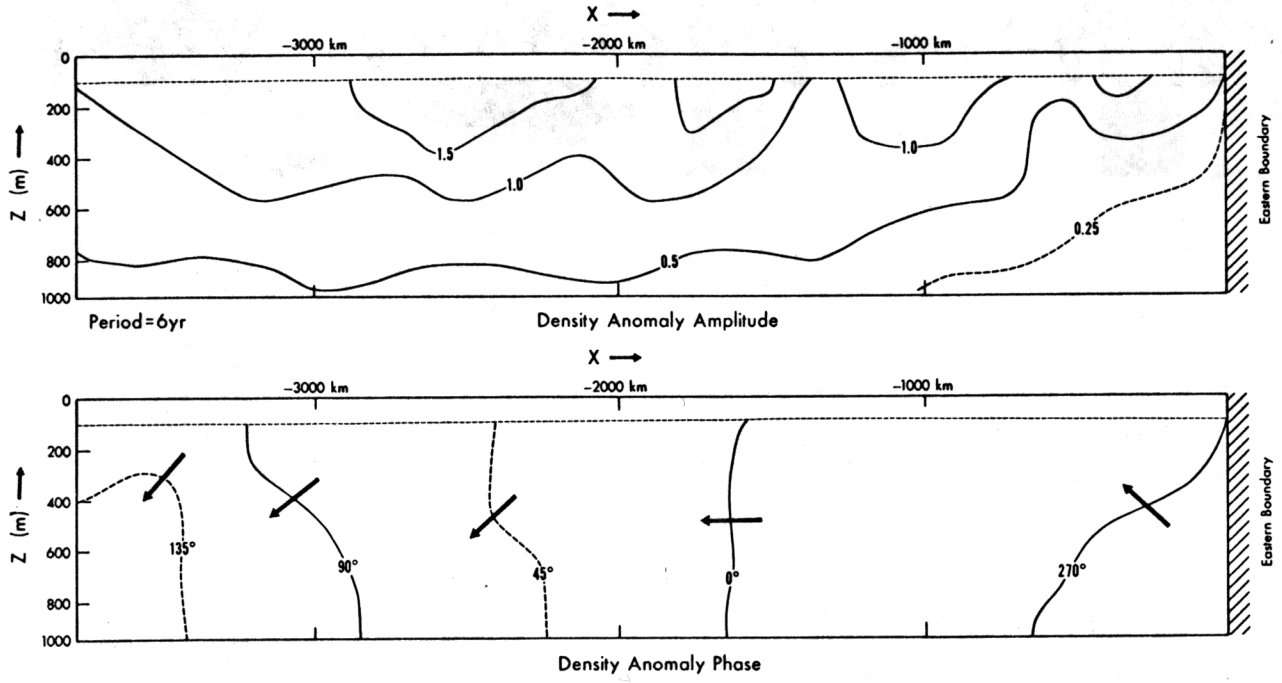

Fig. 9. Same as Figure 6 for a westward moving wind pattern.

tern shows the ocean response to the vicinity of the eastern boundary. Comparing Figure 9 to Figures 6 and 7 we see that there are no amphidromic points. Some weak downward propagation exists well out from the boundary, and upward propagation near the wall, but the dominant feature is westward propagation. For the same wind stress the westward moving wave has a much greater amplitude at depth than the eastward wave.

To simplify the consideration of the standing wave pattern in wind stress, we first consider the case without an eastern wall in Figure 10. The eastward and westward moving waves are equal in amplitude at the base of the mixed layer. The standing pattern of the wind curl is centered at −1000 km. The wavelength of the wind pattern is the same as that shown in Figures 6, 7, and 9. Note that even in the absence of reflected baroclinic waves there is a variation of phase in the vertical. It is such that there is upward propagation east of the wind gyre and downward propagation west of the wind gyre. It is much weaker than it is in the case of an isolated eastward forced wave, however. The formula for the phase angle is

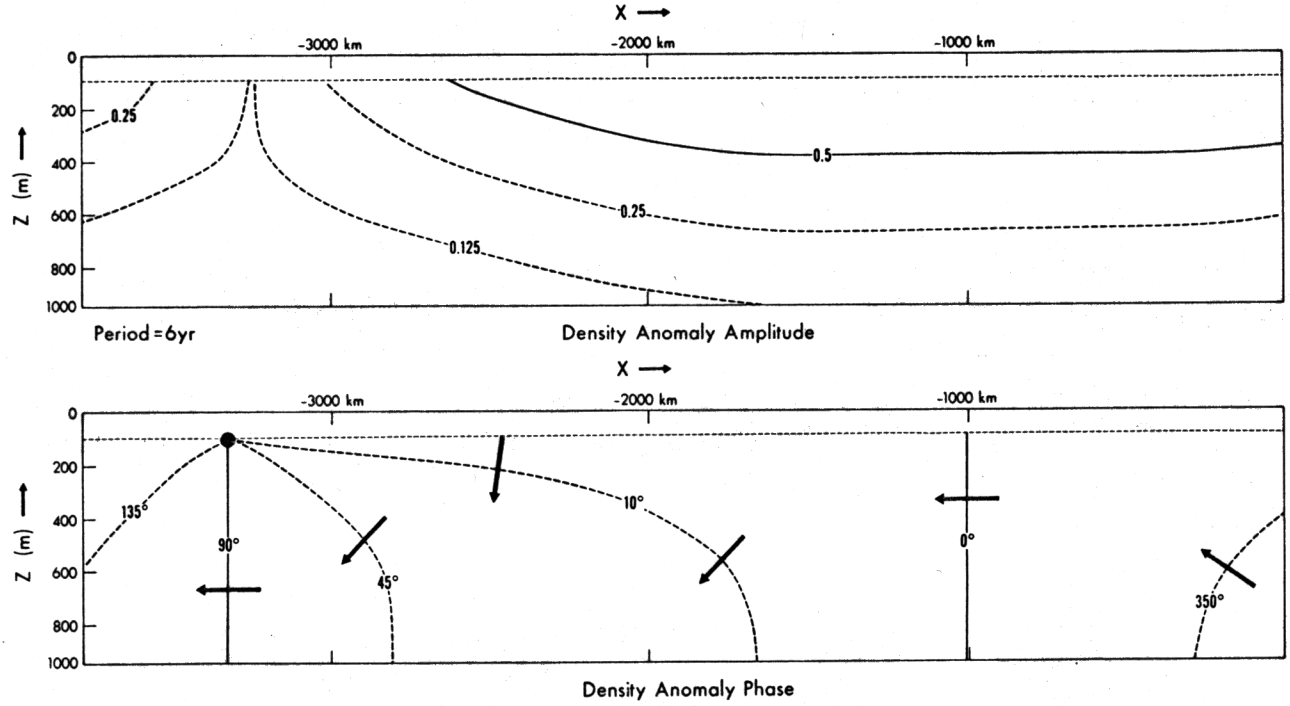

Fig. 10. A standing wave pattern forces an ocean without an eastern or western boundary.

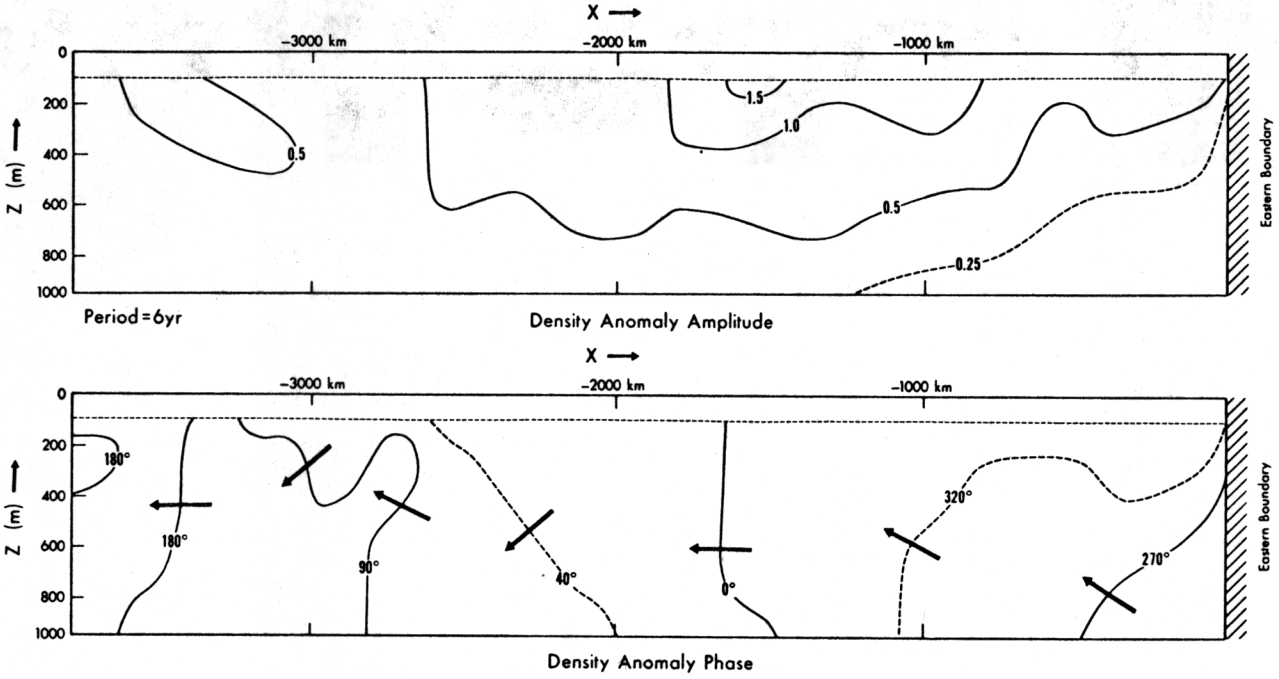

Fig. 11. A standing wind pattern forces an ocean with an eastern boundary.

$$\phi(x, z) = \arctan [F(z) \tan |k_f| (x - x_0)] \qquad (46)$$

where

$$F(z) = (\hat{w}_{f+} - \hat{w}_{f-})/(\hat{w}_{f+} + \hat{w}_{f-}) \qquad (47)$$

At the base of the mixed layer the eastward and westward components are exactly equal and $F(z)$ is zero. At greater depths, however, $F(z)$ becomes negative, since the eastward forced component shown in Figure 3 attenuates very rapidly with depth in relation to the westward forced component, which has a profile very much like that of the first baroclinic mode shown in Figure 4.

Finally, we consider the effect of a standing wave pattern in the wind in the presence of an eastern boundary. The pattern shown in Figure 11 is a distorted version of Figure 10. The main difference is that the amplitude is zero at the wall as required by the geostrophic boundary condition, and the isoline of zero phase is shifted westward. Downward propagation west of the center of the gyre is more intense than it is in Figure 10 but not as striking as it is in Figures 6 and 7, where amphidromic points are present.

CONCLUSIONS

On the assumption that the large-scale temperature anomalies of the North Pacific are primarily associated with large displacements of the thermocline caused by wind, the goal of the present study is to investigate the vertical structure of the anomalies. The long-term temperature records of OWS stations N and P in the eastern North Pacific indicate a curious downward propagation of thermal anomalies at low frequencies. The explanation of this phenomenon formed a primary motivation for this model study.

A simple linear model with horizontally uniform stratification is formulated. It consists of a mixed layer of uniform density and an exponential density profile in the main thermocline. The dynamics are quasi-geostrophic. Since the statistics of low-frequency wind variations over the North Pacific are not well known, several different patterns of wind driving were tested. In one case, only an eastward moving train of wind gyres is considered. The eastward moving wind gyres generate an anomaly in the thermocline that is reflected when it reaches the eastern wall of the model. The reflected waves take the form of large-scale internal Rossby waves. For a reasonable choice of parameters the reflected waves move much more slowly than the incoming wave. Since these long waves are approximately nondispersive, the same is true of the group velocities of the incoming and outgoing waves. If we invoke friction, the higher-mode baroclinic modes will be attenuated before penetrating very far from the western boundary. This provides a mechanism for energy accumulation, since the scattered waves will not be able to carry away all the energy associated with the forced wave. The mechanism is similar in certain respects to *Pedlosky*'s [1965] theory of western intensification. Our simplified model predicts that an incoming warm anomaly added to the scattered outgoing waves would produce an anomalous southward current, while an incoming cold anomaly would have the opposite effect.

For a frequency of $\frac{1}{8}$ cpy, superposition of a forced eastward wave and free outgoing waves produce downward phase propagation at a distance of 2000–2500 km from the eastern boundary. This mechanism is offered as a possible explanation of the observed downward propagation of low-frequency temperature anomalies at OWS stations N and P noted by *White and Walker* [1974]. An alternative explanation of the downward propagation of the temperature anomaly at OWS station N is a local mechanism based on vertical mixing. Periodic temperature variations at the upper boundary of a uniformly conductive ocean will generate anomalies that will move slowly downward at a uniform phase speed dependent on frequency and vertical mixing. This mechanism is explored in appendix B. It is not difficult to show that the vertical mixing required to propagate an anomaly downward at the observed speed of 100 m/yr is in excess of 10^{-4} m^2/s, a much larger value than that indicated by recent measurements of the Cox number reported by *Gregg* [1977].

Forced westward waves produce fairly uniform westward

propagation throughout the water column. Amphidromic points in the x-z plane which are associated with eastward moving forced waves are eliminated. The superposition of eastward and westward moving wind patterns to form a standing wave pattern also causes westward propagation through most of the water column below the mixed layer. In addition, there is upward propagation east of the center of the standing wind pattern and downward propagation to the west.

Future research is indicated along several lines. The work of *Barnett* [1977] on wind stress patterns should be extended to determine the relative importance of eastward and westward incoherent traveling waves versus standing waves in the wind pattern at low frequencies. Model studies using numerical methods could be used to test the validity of the drastic simplifications of the present linear model with uniform stratification. Finally, the historical temperature records for the eastern North Pacific have not been completely analyzed. *Emery and Magaard* [1976] have done an excellent analysis of mid-ocean data, showing that the records are consistent with baroclinic Rossby waves propagating to the northwest. The long-term baththermograph sections between California and Hawaii offer further opportunities for analysis.

Appendix A

In this appendix the boundary condition at the eastern wall is investigated in more detail. The approach is to examine the linear problem in a general way and to determine the conditions for which the geostrophic approximation is justified. Assuming solutions proportional to $\exp(-i\omega t)$ and neglecting the effects of stresses in the mixed layer, we find that (1) and (2) may be combined to form the following expression for u:

$$\rho_0(f^2 - \omega^2)u = i\omega\,\partial_x p - f\,\partial_y p \tag{A1}$$

At the eastern wall the left-hand side of (A1) must vanish. In general, the right-hand side of (A1) must be satisfied by a combination of the forced solution and free baroclinic Rossby waves and Kelvin waves. We have assumed that the wind next to the boundary is zero, so that no local wind-induced upwelling takes place at the coast. For a 'switch on' problem, Kelvin waves would be important, but in the case of low frequency (1 cpy or less), only Rossby waves have the appropriate range of wavelength and frequency to match the incoming wave.

As long as we are concerned only with lower modes, Kelvin waves may be eliminated and the solution written in the following form:

$$p = \sum_{n=0}^{\infty} \gamma_n \hat{p}_n(z) \cos ly \exp\left[i(k_f x - \omega t)\right] + \sum_{n=0}^{\infty} (\alpha_n \cos ly + \beta_n \sin ly)\hat{p}_n(z) \exp\left[i(k_n x - \omega t)\right] \tag{A2}$$

Parameter γ_n is the amplitude of the forced solution projected onto the normal modes. The free waves are written in a way to allow for both a sin ly and a cos ly component. Substituting (A2) into the right-hand side of (A1) and setting the left-hand side of (A1) equal to zero, we obtain

$$\begin{bmatrix} \omega k_n & fl \\ fl & -\omega k_n \end{bmatrix} \begin{bmatrix} \alpha_n \\ \beta_n \end{bmatrix} = \begin{bmatrix} -\omega k_f \gamma_n \\ -fl\gamma_n \end{bmatrix} \tag{A3}$$

Let

$$C_n,\ C_f,\ U = \omega/k_n,\ \omega/k_f,\ \omega^2/fl \tag{A4}$$

The solution of (A3) may be written

$$\alpha_n = -\gamma_n \frac{(1 + U^2/C_n C_f)}{(1 + U^2/C_n^2)} \tag{A5}$$

$$\beta_n = -\gamma_n \frac{(U/C_f - U/C_n)}{(1 + U^2/C_n^2)} \tag{A6}$$

The quantity U varies from 0.04 km/day for a period of 1 year to 0.001 km/day for a period of 6 years. The geostrophic boundary condition corresponds to $\alpha_n = -\gamma_n$ and $\beta_n = 0$. It can be justified if $U \ll C_f$ and $U \ll |C_n|$. These conditions are very well satisfied (see Table 2) by the first four modes which account for most of the variance of the reflected wave. For the higher modes the nongeostrophic term would cause a slight southward phase shift of the reflected wave in relation to the incoming wave.

Appendix B

In what follows we wish to explore an alternative hypothesis to explain the downward penetration of temperature anomalies at OWS station N. If we assume that vertical mixing is solely responsible for the downward propagation of 100 m/yr noted by *White and Walker* [1974], the governing equation would be

$$\partial_t T' - (\kappa/2)\partial_z \partial_z T' = 0 \tag{B1}$$

The boundary conditions may be specified as

$$T' = T_0 \qquad z = 0 \tag{B2}$$

and

$$T' = 0 \qquad z = -\infty \tag{B3}$$

(B1)–(B3) are satisfied by a solution of the form

$$T' = T_0 \exp\left[(\omega/\kappa)^{1/2}(1 - i)z - i\omega t\right] \tag{B4}$$

The vertical phase speed of the thermal anomaly will be

$$C_{ph} = -(\omega\kappa)^{1/2} \tag{B5}$$

A value for $\kappa/2$ of 1.5×10^{-4} m^2 s^{-1} would be required to match the dominant period of 6 years and the phase speed of 100 m/yr noted by *White and Walker* [1974]. We can compare this value with direct measurements of the Cox number recently reported by *Gregg* [1977]. Gregg summarizes data taken at several different seasons at 28°N and 155°W not far from OWS station N. His measurements indicate peak values of vertical mixing in winter, but even at that season the implied vertical mixing in only 0.5×10^{-5} m^2/s or less than 1 order of magnitude than the vertical mixing required for the observed speed of vertical propagation of North Pacific temperature anomalies.

Acknowledgments. The authors are deeply grateful for stimulating discussions with George Philander, Warren White, and David Anderson. Warren White kindly made available to us a preprint of his paper [*White*, 1977]. Martha Jackson and Elizabeth Williams provided essential assistance in evaluating the solutions and preparing the manuscript.

References

Abramowitz, M., and I. A. Stegun, *Handbook of Mathematical Functions*, U. S. Government Printing Office, Washington, D. C., 1964.

Barnett, T. P., The principal time and space scales of the Pacific trade wind fields, *J. Atmos. Sci., 34*, 221–236, 1977.

Davis, R. E., Predictability of sea surface temperature and sea level pressure anomalies over the North Pacific Ocean, *J. Phys. Oceanogr., 6*, 249–266, 1976.

Emery, W. J., and L. Magaard, Baroclinic Rossby waves as inferred

from temperature fluctuations in the Eastern Pacific, *J. Mar. Res., 34,* 365–385, 1976.
Favorite, F., and D. McLain, Coherence in transpacific movements of positive and negative anomalies of sea surface temperature, 1953–60, *Nature, 244,* 139–143, 1973.
Fofonoff, N. P., and S. Tabata, Variability of oceanographic conditions between ocean station 'P' and Swiftsure Bank off the Pacific Coast of Canada, *J. Fish. Res. Bd. Can., 28,* 825–868, 1966.
Garrett, C., and W. Munk, Space-time scales of internal gravity waves, *Geophys. Fluid Dyn., 3,* 225–264, 1972.
Gregg, M. C., Variations in the intensity of small-scale mixing in the main thermocline, *J. Phys. Oceanogr., 7,* 436–454, 1977.
Hasselmann, K., and C. Frankignoul, Stochastic forcing of the upper ocean, *Tellus,* in press, 1977.
Namias, J., Thermal communication between sea surface and the lower troposphere, *J. Phys. Oceanogr., 3,* 373–378, 1973.
Pedlosky, J., A note on the western intensification of the oceanic circulation, *J. Mar. Res., 23,* 207–209, 1965.
Veronis, G., and H. Stommel, The action of variable wind stresses on a stratified ocean, *J. Mar. Res., 15,* 43–75, 1956.
White, W. B., SST anomaly development and baroclinic long waves in the North Pacific current, *Norpax Highlights, 3*(1), 2–4, 1975.
White, W. B., Annual forcing of baroclinic long waves in the tropical North Pacific Ocean, *J. Phys. Oceanogr., 7,* 50–61, 1977.
White, W. B., and A. E. Walker, Time and depth scales of anomalous subsurface temperatures of Ocean Weather Stations P, N, and V in the North Pacific, *J. Geophys. Res., 79,* 4517–4522, 1974.

(Received March 17, 1977;
revised October 11, 1977;
accepted October 17, 1977.)